Mathematical analysis of magnetohydrodynamic (MHD) flow of micropolar nanofluid under buoyancy effects past a vertical shrinking surface: dual solutions

Liaquat Ali Lund [a,b], Zurni Omar [a], Ilyas Khan [c,*]

[a] *School of Quantitative Sciences, Universiti Utara Malaysia, Sintok, 06010, Kedah*
[b] *KCAET Khairpur, Sindh Agriculture University, Tandojam Sindh, Pakistan*
[c] *Faculty of Mathematics and Statistics, Ton Duc Thang University, Ho Chi Minh City, Viet Nam*

ARTICLE INFO

ABSTRACT

In this paper, we explore dual solutions of MHD flow, heat and mass transfer of micropolar nanofluid over a linear vertical shrinking surface with buoyancy effects, which was not considered in the previous works. The governing fluid flow equations of this problem are transformed into nonlinear boundary value problems (BVPs) of ordinary differential equations (ODEs) by applying similarity variables. The resultant BVPs are converted into initial value problems (IVPs) by using shooting method which then resolved by employing Runge Kutta of order four. The impacts of the governing parameters, such as suction parameter, material parameter, Richardson number, magnetic parameter, Prandtl number, thermophoresis and Brownian motion parameters on velocity, angular velocity, temperature, and concentration are illustrated graphically. The results indicate that the existence of a range of dual solutions and no-solutions. When Richardson number (δ) is increased, the reduction of the velocity of micropolar nanofluid has occurred in the second solution. The stability analysis on dual solutions, however, reveals that only the first solution is stable.

1. Introduction

Eringen [2] was the primary researcher who presented a simple concept of micropolar fluid and its characteristics. He expanded his research and wrote an article, after two years, in which compressive investigation of micropolar had been given (see [3]). At the end of the twentieth, century, Lukaszewicz [4] composed a comprehensive book on micropolar fluid and broke it down in details. Micropolar fluid is a polar fluid which contains spherical or rigid randomly oriented particles. It can be defined as a fluid with microstructures and belongs to the nonsymmetric stress tensor. Some common instances of micropolar fluid are liquid crystals, liquids of bubby, and animal blood [5]. Damseh et al. [6] studied the effect of chemical reaction of micropolar fluid in presence of heat generation on the stretching sheet and found that non-Newtonian parameter effect was directly proportional to the skin friction coefficient. Electrical MHD flow of micropolar nanofluid was examined by Chamkha et al. [7]. Meanwhile, Magyari et al. [8] considered micropolar fluid and concluded that temperature decreased when heat absorption parameter was increased. Hayat et al. [1] considered micropolar

nanofluid with thermal radiation effect using of Buongiorno model. The recent development of micropolar nanofluid can be referred to the work done by [9, 10, 11, 12, 13, 14]. One of the main objectives of this study is to expand the work of Hayat et al. [1] and Haq et al. [10] for multiple solutions of micropolar nanofluid without consideration of thermal radiation effect on a vertical shrinking sheet.

Boundary layer flow of shrinking and stretching sheets have vast applications in manufacturing process and engineering, particularly in metallurgy and polymer industry [15]. Other applications of boundary layer flow might be found in aerodynamics continuous glass casting, metal extrusion, extrusion of plastic sheets, glass fiber production, extraction of polymer, and sheet hot rolling of textiles. Crane [16] was the pioneer who considered similarity solution for stretching surface and found an exact analytic solution. He also investigated the thermal approach to this problem [17]. Since then, the study of boundary layer flow of shrinking sheet has gained popularity. Miklavčič and Wang [18] had developed a model of viscous flow on a shrinking surface first time. Their work has then been extended by numerous researchers [19, 20, 21, 22, 23].

---

* Corresponding author.
    E-mail address: ilyaskhan@tdtu.edu.vn (I. Khan).

Rapidly changing technologies are the characteristics of the present century and this trend will continue. Currently, it can be seen that researchers, mathematicians, and scientists are trying to understand the principles of fluid mechanics extensively in order to implicate them in many different practical problems [24, 25, 26, 27]. Biomedical, aeronautical, mechanical, civil, and marine engineers as well as geophysicists, astrophysicist, meteorologists, space researchers, mathematicians, physicists physical, and oceanographers had used this knowledge to handle a huge number of complex flow phenomena. The last two and half decades are also witnessing a great surge in the use convective fluids for heat transfer such as minerals ethylene glycol, oil and water assume an imperative part in numerous industry segments such as chemical production, microelectronics, power generation, transportation, and air-conditioning. Nanofluid is a new class of heat transfer fluid which contains base fluid with nanoparticles of sized 1–100nm. Nanofluid has high thermal conductivity as compared to base fluid [28]. Choi [29] was the first who gave the concept of improvement of heat transport by mixing solid particles of nanometer-sized in base water. These particles are made of nonmetals (nanotubes, graphite, carbon), carbides (SiC), chemically stable metals (Ag, Cu, Au, Al, Fe), oxides ceramics (SiO2, CuO, Al2O3, TiO2), PCM, nitrides (SiN, AlN), layered (Cu + C, Al + Al2O3), and functionalized nanoparticles [30]. There are only two models that support transport phenomena. The first one is known as Buongiorno model [31] which is a two-phase model and described as velocity of flow is the sum of base fluid and the slip velocity. The second one is called as Tiwari and Das's model [32] which is a single-phase model and described as thermophysical properties as functions of nanoparticle volume fraction. Turkyilmazoglu [33] used Buongiorno model to examine the effect of thermophoresis effect on nanofluid. Cu-water based nanofluid was considered by Chamkha et al. [34] and they claimed that the entropy generation and Nusselt number were decreased when the volume fraction was increased. Many other researchers also considered these models in their studies [35, 36, 37].

Convection occurs when the heat is transferred through fluids (gases or liquids). In this process, heat dependably exchanges from a hotter spot to a cooler spot. The convective transfer of heat is only depending on the nature of the flow. Convection has three modes namely forced, natural (free) and mixed convection. Forced convection can be defined as a mechanism or mode of heat transport in which fluid motion is generated by an external source. Examples of forced convection are a fan, suction device and pump and so forth. On the other hand, natural convection is a process where heat is transferred by density variances in the fluid occurring because of gradients of temperature. It happens because of the temperature contrasts which affect the fluid density. It is not created by external sources and also referred as free convection. Due to important applications of natural convection in various fields of engineering, many researchers considered it in their studies. Bourantas et al. [38] considered micropolar nanofluid over an inclined plane with the bouncy effect. Micropolar nanofluid has been examined by Bourantas and Loukopoulos [39] theoretically with the effect of natural convection and found that the increase in nanoparticles micro-rotation caused the decline in the heat transfer rate. Recently, many researchers likewise developed micropolar or Newtonian models for natural convection of nanofluids [refer, 9, 40, 41, 42, 43, 44].

This study is an extension of work done by Hayat et al. [1] over a vertical shrinking surface which was not considered in their studies. In addition, we also extend it for MHD and multiple solutions since Haq et al. [10] did not consider the MHD effects on micropolar nanofluid. Therefore, the prime objective of this research is to find all possible multiple solutions of MHD flow of micropolar nanofluid under the described circumstances. We anticipate that these findings will provide the fruitful help to enhance the development of technology and science in the future.

2. Materials & methods

Numerical study of micropolar nanofluid over a vertical linear shrinking surface with the effect of magnetic has been investigated. All assumptions of the problem can be seen in Fig. 1. The field velocities in directions of x and y are denoted by u and v respectively. N, T and C represent the microrotation, temperature and volume friction of nanoparticles within the boundary layer, respectively. Meanwhile, T_w indicates the temperature of fluid and and C_w is the volume friction of nanoparticles at the wall. In the case when both parameters are away from the wall, they are represented by T_∞ and C_∞, respectively. It is assumed that the uniform intensity of magnetic force is acted normally to the plane of the surface. Along with all mentioned conditions, the governing equations of continuity, momentum, angular momentum, temperature and concentration can be written in the Buongiorno model [31] as below

$$\nabla \cdot \boldsymbol{V} = 0 \tag{1}$$

$$\rho_f \frac{d\boldsymbol{V}}{dt} = -\nabla \boldsymbol{P} + (\mu_f + \kappa)\nabla^2 \boldsymbol{V} + \kappa(\nabla \times \boldsymbol{N}) + (\boldsymbol{J} \times \boldsymbol{B})$$
$$+ \left[(1 - C_\infty)\rho_{f_\infty}\beta(T - T_\infty) - (\rho_p - \rho_{f_\infty})(C - C_\infty)\right]\mathbf{g} \tag{2}$$

$$\rho_f j \frac{d\boldsymbol{N}}{dt} = \gamma \nabla^2 \boldsymbol{N} - \kappa(2\boldsymbol{N} - \nabla \times \boldsymbol{V}) \tag{3}$$

$$(\rho c)_p \frac{dT}{dt} = k\nabla^2 T + (\rho c)_f \left[D_B \nabla C . \nabla T + \frac{D_T}{T_\infty}(\nabla T)^2\right] \tag{4}$$

$$\frac{d\boldsymbol{C}}{dt} = D_B \nabla^2 C + \frac{D_T}{T_\infty}\nabla^2 T \tag{5}$$

where the velocity vector is $\boldsymbol{V} \equiv [u(x,y), v(x,y), 0]$, the microrotation vector is N, the magnetic field strength is $\boldsymbol{B} \equiv [0, B_0, 0]$, the spin gradient viscosity is γ, density of current is $\boldsymbol{J} \equiv \sigma^*(\boldsymbol{V} \times \boldsymbol{B})$, micro-rotation viscosity coefficient is κ, the gravitational acceleration is $\mathbf{g} \equiv [0, g, 0]$, micro-inertia density is $j, \mu_f, p, \rho_p, \rho_f, k, D_B, D_T(\rho c)_p$, and $(\rho c)_f$ stand for base fluid viscosity, pressure, the nanoparticle material densities, densities of base fluid, the thermal conductivity, the coefficient of Brownian motion, the thermophoretic diffusion coefficient, the effective heat capacity of the nanoparticle material, and the effective heat capacity of the base fluid, respectively.

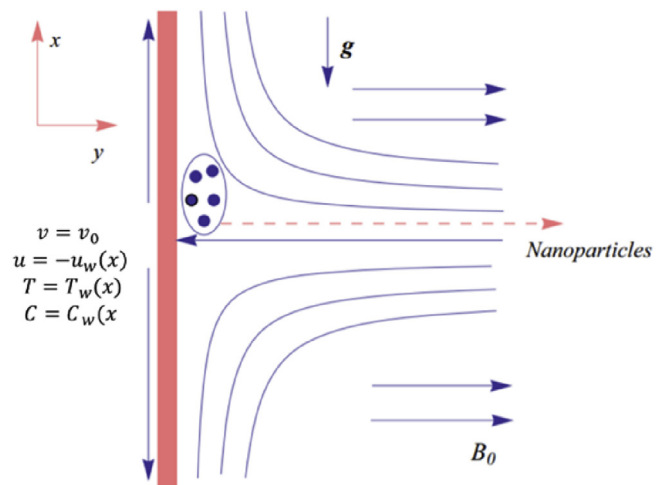Applying scale analysis, resulting boundary layer equations are obtained:

Fig. 1. Diagram of flow problem and coordinate system.

$$\frac{\partial u}{\partial x} + \frac{\partial v}{\partial y} = 0 \tag{6}$$

$$u\frac{\partial u}{\partial x} + v\frac{\partial u}{\partial y} = \left(\vartheta_f + \frac{\kappa}{\rho}\right)\frac{\partial^2 u}{\partial y^2} + \frac{\kappa}{\rho_f}\frac{\partial N}{\partial y} - \frac{\sigma^* B_0^2 u}{\rho_f}$$
$$+ \frac{1}{\rho_f}\left[(1 - C_\infty)\rho_{f_\infty}\beta(T - T_\infty) - (\rho_p - \rho_{f_\infty})(C - C_\infty)\right]g \tag{7}$$

$$u\frac{\partial N}{\partial x} + v\frac{\partial N}{\partial y} = \frac{1}{\rho j}\left[\gamma\frac{\partial^2 N}{\partial y^2} - \kappa\left(2N + \frac{\partial u}{\partial y}\right)\right] \tag{8}$$

$$u\frac{\partial T}{\partial x} + v\frac{\partial T}{\partial y} = \alpha_f\frac{\partial^2 T}{\partial y^2} + \tau_w\left[D_B\frac{\partial C}{\partial y}\frac{\partial T}{\partial y} + \frac{D_T}{T_\infty}\left(\frac{\partial T}{\partial y}\right)^2\right] \tag{9}$$

$$u\frac{\partial C}{\partial x} + v\frac{\partial C}{\partial y} = D_B\frac{\partial^2 C}{\partial y^2} + \frac{D_T}{T_\infty}\frac{\partial^2 T}{\partial y^2} \tag{10}$$

subject to boundary conditions

$$v = v_0; u = -u_w(x); N = -m\frac{\partial u}{\partial y}; T = T_w; C = C_w \ \text{at} \ y = 0$$

$$u \to 0; N \to 0; T \to T_\infty; C \to C_\infty \ \text{as} \ y \to \infty \tag{11}$$

For the current problem, we have following dimensionless similarity variables

$$\eta = y\sqrt{\frac{a}{\vartheta_f}}, u = axf'(\eta), v = -\sqrt{a\vartheta_f}f(\eta), N = \sqrt{\frac{a}{\vartheta_f}}axg(\eta), \theta(\eta) = \frac{(T - T_\infty)}{(T_w - T_\infty)},$$
$$\varnothing(\eta) = \frac{(C - C_\infty)}{C_\infty}, \tag{12}$$

Substituting Eq. (12) in Eqs. (6), (7), (8), (9), and (10), the equation of continuity is contented automatically and the remaining Eqs. (7), (8), (9), and (10) are assumed to be in the following forms

$$(1 + K)f''' + ff'' - f'^2 + Kg' - Mf' + \delta(\theta - N_r\varnothing) = 0 \tag{13}$$

$$\left(1 + \frac{K}{2}\right)g'' + fg' - gf' - 2Kg - Kf'' = 0 \tag{14}$$

$$\frac{1}{Pr}\theta'' + f\theta' + N_b\varnothing'\theta' + N_t(\theta')^2 = 0 \tag{15}$$

$$\frac{1}{Sc}\varnothing'' + f\varnothing' + \frac{1}{Sc}\frac{N_t}{N_b}\theta'' = 0 \tag{16}$$

with boundary conditions below

$$f(0) = f_w, f'(0) = -1, g(0) = -mf''(0), \ \theta(0) = 1, \ \varnothing(0) = 1$$

$$f'(\eta) \to 0; g(\eta) \to 0; \theta(\eta) \to 0; \ \varnothing(\eta) \to 0 \ as \eta \to \infty \tag{17}$$

where K is the micropolar material parameter, M is the Hartmann number, δ is the parameter of local mixed convection or Richardson number which depends on the x independent variable. Therefore, the problem can be considered as a local similar. It is worth to note that $\delta < 0, \delta > 0$ and $\delta = 0$ indicate a cooled surface, a hot surface and a forced convection flow, respectively. N_r is the buoyancy ratio parameter, Pr and Sc are the Prandtl and Schmidt numbers respectively, N_t and N_b are the thermophoresis and Brownian diffusion parameters respectively. Suction/blowing parameter is f_w, m is the micro-gyration parameter. The above all parameters can be expressed as:

$$\begin{cases} K = \dfrac{\kappa}{\mu}, M = \dfrac{\sigma^* B_0^2}{\rho_f a}, \delta = \dfrac{g\beta(1 - C_\infty)(T_w - T_\infty)}{a^2 x}, \\[2mm] N_r = \dfrac{(\rho_p - \rho_{f_\infty})C_\infty}{\rho_{f_\infty}\beta(1 - C_\infty)(T_w - T_\infty)}, Pr = \dfrac{\vartheta_f}{\alpha_f}, Sc = \dfrac{\vartheta_f}{D_B} \\[2mm] N_t = \dfrac{\tau_w D_T(T_w - T_\infty)}{\vartheta_f T_\infty}, N_b = \dfrac{\tau_w D_B C_\infty}{\vartheta_f}, f_w = -\dfrac{v_0}{\sqrt{a\vartheta_f}} \end{cases} \tag{18}$$

The physical quantities of interests are Skin friction coefficient C_f, local Nusselt number N_u, and Sherwood number S_h, which can be expressed as

$$C_f = \frac{\left[(\mu + \kappa)\frac{\partial u}{\partial y} + \kappa N\right]_{y=0}}{\rho u_w^2}, N_u = \frac{-x\left[\frac{\partial T}{\partial y}\right]_{y=0}}{(T_w - T_\infty)}, S_h = \frac{-x\left(\frac{\partial C}{\partial y}\right)_{y=0}}{C_\infty} \tag{19}$$

Using Eq. (7) in (13), we get

$$C_f(Re_x)^{\frac{1}{2}} = (1 + (1-m)K)f''(0), N_u(Re_x)^{-\frac{1}{2}} = -\theta'(0), S_h(Re_x)^{-\frac{1}{2}} = -\varnothing'(0) \tag{20}$$
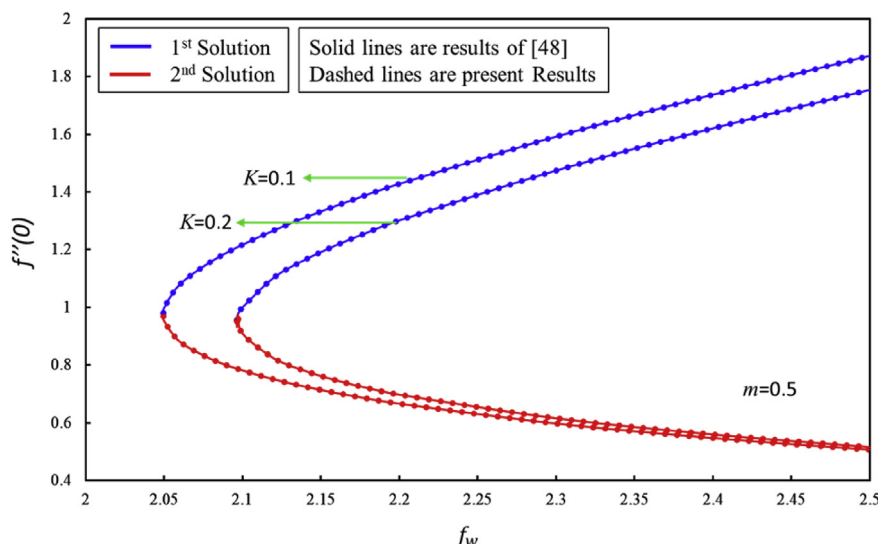

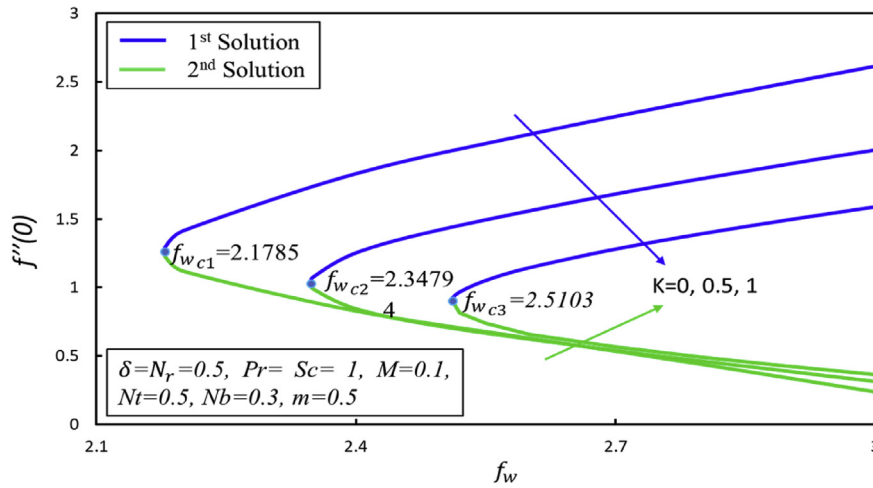**Fig. 2.** Comparison of $f'(0)$ with results of [48], when $m = 0.5, M = 0$ and $\delta = 0$.

Fig. 3. Coefficient of Skin friction $f''(0)$ versus the suction f_w for varying material parameter K.

where $Re_x = ax^2/\vartheta_f$ is local Reynolds number.

3. Analysis

3.1. Stability analysis

In the case where multiple solutions exist in any boundary layer problems, it is necessary to investigate which solution is a stable solution (upper or first solution) and physically possible. Although only stable solution has different applications in various field, unstable solutions also should be considered from a mathematical point of view as it cannot be seen experimentally. This is due to the fact that they are also part of the same problem and fulfill all the requirements of the solution.

For the current problem, dual solutions in a range of different parameters were successfully found. In order to indicate an upper solution from them, we need to consider the unsteady model of the problem, which can be expressed as

$$\frac{\partial u}{\partial t} + u\frac{\partial u}{\partial x} + v\frac{\partial u}{\partial y} = \left(\vartheta_f + \frac{\kappa}{\rho}\right)\frac{\partial^2 u}{\partial y^2} + \frac{\kappa}{\rho_f}\frac{\partial N}{\partial y} - \frac{\sigma^* B_0^2 u}{\rho_f}$$
$$+ \frac{1}{\rho_f}\left[(1 - C_\infty)\rho_{f_\infty}\beta(T - T_\infty) - (\rho_p - \rho_{f_\infty})(C - C_\infty)\right]g \quad (21)$$

$$\frac{\partial N}{\partial t} + u\frac{\partial N}{\partial x} + v\frac{\partial N}{\partial y} = \frac{1}{\rho j}\left[\gamma\frac{\partial^2 N}{\partial y^2} - \kappa\left(2N + \frac{\partial u}{\partial y}\right)\right] \quad (22)$$

$$\frac{\partial T}{\partial t} + u\frac{\partial T}{\partial x} + v\frac{\partial T}{\partial y} = \alpha_f\frac{\partial^2 T}{\partial y^2} + \tau_w\left[D_B\frac{\partial C}{\partial y}\frac{\partial T}{\partial y} + \frac{D_T}{T_\infty}\left(\frac{\partial T}{\partial y}\right)^2\right] \quad (23)$$

$$\frac{\partial C}{\partial t} + u\frac{\partial C}{\partial x} + v\frac{\partial C}{\partial y} = D_B\frac{\partial^2 C}{\partial y^2} + \frac{D_T}{T_\infty}\frac{\partial^2 T}{\partial y^2} \quad (24)$$

where time is denoted by t. The following new similarity transformation variables are applied in Eqs. (21), (22), (23), and (24)

$$\eta = y\sqrt{\frac{a}{\vartheta_f}}, \tau = at, u = ax\frac{\partial f(\eta, \tau)}{\partial \eta}, v = -\sqrt{a\vartheta_f}f(\eta, \tau), N = \sqrt{\frac{a}{\vartheta_f}}axg(\eta, \tau),$$

$$\theta(\eta, \tau) = \frac{(T - T_\infty)}{(T_w - T_\infty)}, \varnothing(\eta, \tau) = \frac{(C - C_\infty)}{C_\infty}, \quad (25)$$

which leads to

$$(1 + K)\frac{\partial^3 f}{\partial \eta^3} + f\frac{\partial^2 f}{\partial \eta^2} - \left(\frac{\partial f}{\partial \eta}\right)^2 + K\frac{\partial g}{\partial \eta} - M\frac{\partial f}{\partial \eta} + \delta(\theta - N_r\varnothing) - \frac{\partial^2 f}{\partial \tau \partial \eta} = 0 \quad (26)$$

$$\left(1 + \frac{K}{2}\right)\frac{\partial^2 g}{\partial \eta^2} + f\frac{\partial g}{\partial \eta} - g\frac{\partial f}{\partial \eta} - Kg - K\frac{\partial^2 f}{\partial \eta^2} - \frac{\partial g}{\partial \tau} = 0 \quad (27)$$
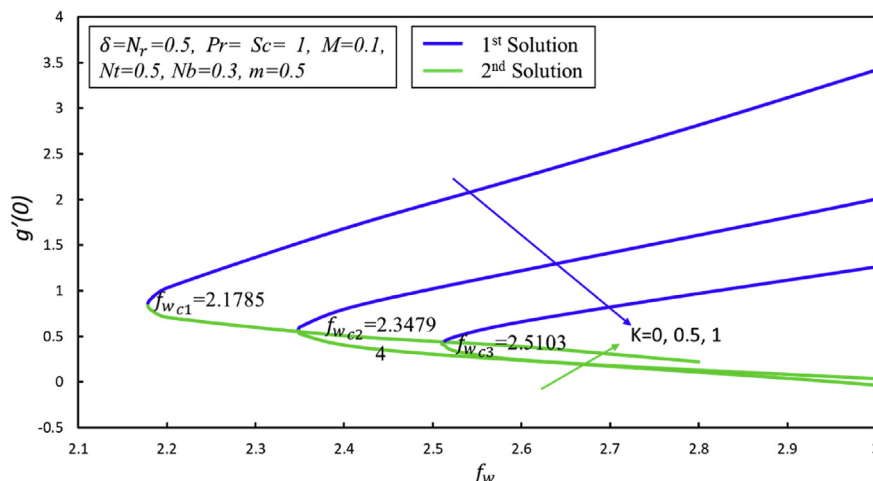

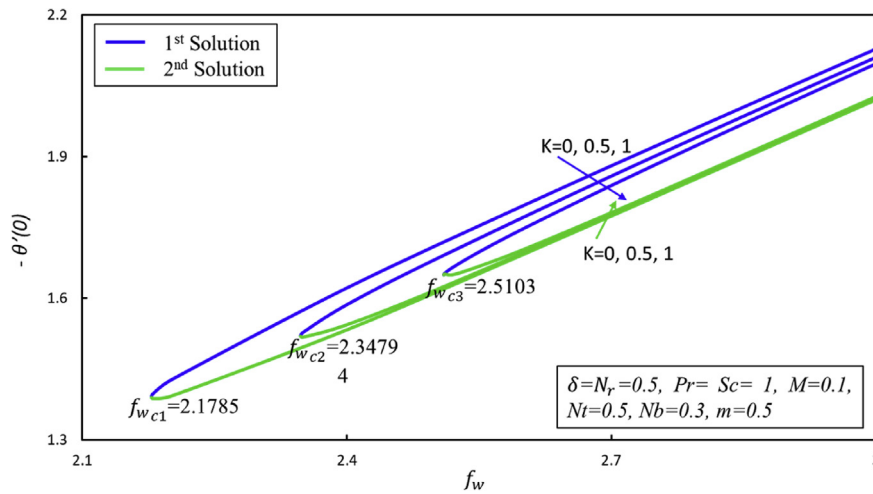**Fig. 4.** Coefficient of couple stress $g'(0)$ versus the suction f_w for varying material parameter K.

Fig. 5. Local Nusselt number $-\theta'(0)$ versus the suction f_w for varying material parameter K.

$$\frac{1}{Pr}\frac{\partial^2\theta}{\partial\eta^2}+f\frac{\partial\theta}{\partial\eta}+N_b\frac{\partial\varnothing}{\partial\eta}\frac{\partial\theta}{\partial\eta}+N_t\left(\frac{\partial\theta}{\partial\eta}\right)^2-\frac{\partial\theta}{\partial\tau}=0 \qquad (28)$$

$$\frac{1}{Sc}\frac{\partial^2\varnothing}{\partial\eta^2}+f\frac{\partial\varnothing}{\partial\eta}+\frac{1}{Sc}\frac{N_t}{N_b}\frac{\partial^2\theta}{\partial\eta^2}-\frac{\partial\varnothing}{\partial\tau}=0 \qquad (29)$$

with the following boundary conditions

$$f(0,\tau)=f_w;\frac{\partial f(0,\tau)}{\partial\eta}=-1;g(0,\tau)=-m\frac{\partial^2 f(0,\tau)}{\partial\eta^2};\theta(0,\tau)=1;\varnothing(0,\tau)=1$$

$$\frac{\partial f(\eta,\tau)}{\partial\eta}\to 0;g(\eta,\tau)\to 0;\theta(\eta,\tau)\to 0;\varnothing(\eta,\tau)\to 0 \text{ as } \eta\to\infty. \qquad (30)$$

According to Lund et al. [21], Merkin [45], Lund et al. [46], and Alarifi et al. [47], these functions/expressions $f(\eta,\tau)=f_0(\eta)+e^{-\varepsilon\tau}F(\eta)$, $g(\eta,\tau)=g_0(\eta)+e^{-\varepsilon\tau}G(\eta)$, $\theta(\eta,\tau)=\theta_0(\eta)+e^{-\varepsilon\tau}H(\eta)$ and $\varnothing(\eta,\tau)=\varnothing_0(\eta)+e^{-\varepsilon\tau}S(\eta)$ are substituted in Eqs. (26), (27), (28), and (29) along boundary condition (30) where ε represents the eigenvalue and $F(\eta)$, $G(\eta)$, $H(\eta)$, and $S(\eta)$ are small relative to $f_0(\eta)$, $g_0(\eta)$, $\theta_0(\eta)$ and $\varnothing_0(\eta)$, respectively. After simplification and by keeping $\tau=0$, we will obtain

$$(1+K)F_0'''+f_0F_0''+F_0f_0''-2f_0'F_0'+KG_0'-MF_0'+\delta(H_0-N_rS_0)+\varepsilon F_0'=0 \qquad (31)$$

$$\left(1+\frac{K}{2}\right)G_0''+f_0G_0'+F_0g_0'-g_0F_0'-g_0'F_0-2KG_0-KF_0''+\varepsilon G_0=0 \qquad (32)$$

$$\frac{1}{Pr}H_0''+f_0H_0'+F_0\theta_0'+N_b\varnothing_0'H_0'+N_bS_0'\theta_0'+2N_t\theta_0'H_0'+\varepsilon H_0=0 \qquad (33)$$

$$S_0''+Sc(f_0\varnothing_0'+F_0S_0')+\frac{N_t}{N_b}H_0''+Sc.\varepsilon S_0=0 \qquad (34)$$

with the boundary conditions

$$F_0(0)=0,F_0'(0)=0,G_0(0)=-mF_0''(0),H_0(0)=0,S_0(0)=0$$

$$F_0'(\eta)\to 0,G_0(\eta)\to 0,H_0(\eta)\to 0,S_0(\eta)\to 0 \text{ as } \eta\to\infty. \qquad (35)$$

To solve the above linearized Eqs. (31), (32), (33), and (34) with boundary conditions (35), BV4C solver function in MATLAB software was employed. In order to find the values of the smallest eigenvalue ε, we have to relax one boundary condition into initial condition as recommended by Lund et al. [21, 46]. For this particular problem, we relaxed the $F_0(\eta)\to 0$ as $\eta\to\infty$ into $F_0'(0)=1$. It should be noted that the negative smallest eigenvalues indicate the initial growth of disturbance, henceforth solution of fluid flow develops instability. In contrast, if the
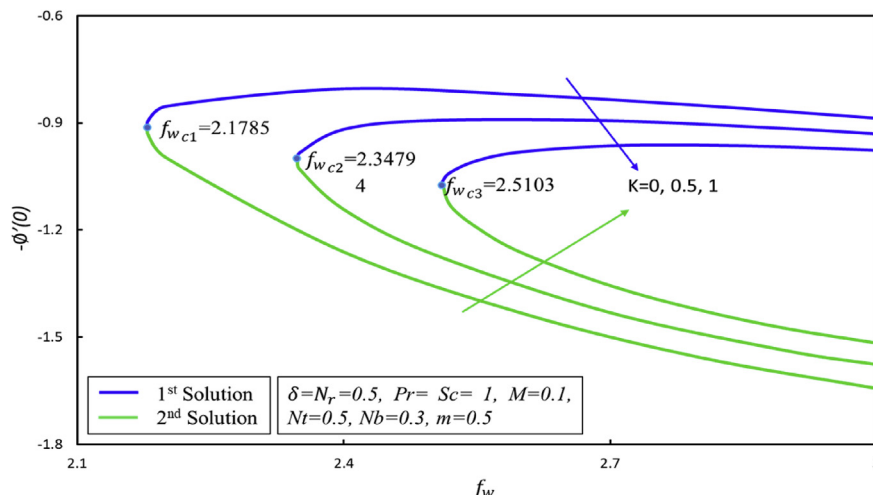

Fig. 6. Local Sherwood number $-\varnothing'(0)$ versus the suction f_w for varying material parameter K.

values of the smallest eigenvalue are positive which means the flow of fluid is stable and physically realizable.

4. Results and discussion

The above Eqs. (13), (14), (15), (16), and (17) are solved by employing shooting method and Runge-Kutta of fourth order in Maple software function i.e. *shootlib* function. For stability analysis, another method called three-stage Lobatto three formula, which is based on finite difference code, developed in *BVP4C* function in MATLAB software was used. According to Lund et al. [21], "this collocation formula and the collocation polynomial provides a C_1 continuous solution that is fourth-order accurate uniformly in *[a,b]*. Mesh selection and error control are based on the residual of the continuous solution". The behavior of central coefficient of the flow can be obtained with the computational simulations of mathematical model.

The numerical analysis has been done for many values of different dominant parameters. It must be noted that the range of thickness of different boundary layer are $\eta_{min_\infty} = 8$ and $\eta_{max_\infty} = 15$ so that the thickness of boundary layers of velocity, angular velocity, concentration and temperature profiles will fulfil boundary conditions asymptotically. To check the accuracy of our method, the results of $f''(0)$ were compared graphically to Bhattacharyya et al. [48] as displayed in Fig. 2 and found in excellent agreements. This accuracy suggests that our methods and their computer coding work properly. The results are demonstrated in terms of coefficient of skin friction, coefficient of couple stress, heat and mass transfer rates. In addition, velocity, angular velocity, temperature, and nanoparticles volume fraction profiles are also examined numerically and graphically. It can be concluded from this analysis that there are ranges of no and dual solutions depending on the values of mass suction f_w and micropolar parameter K as illustrated in Figs. 3, 4, 5, and 6. Fig. 3 was drawn to show the effect of suction on skin friction coefficient for three different values of K. When $K = 0$, there exists the range of no (dual) solution when suction $f_w > 2.1785 (< 2.1785)$. Dual solutions exist for $K = 0.5$ and 1, when the range of $f_w < 2.3479$ and 2.5103 respectively. It is also noticed that high rate of suction is required for non-Newtonian (Micropolar) fluid in order to maintain the flow as compared to the Newtonian fluid. Coefficient of skin friction declines in the first solution as suction increases due to the fact that the increments

in material parameter produce the resistance as a result skin friction decreases. On the other hand, the opposite trend can be seen in the second solution. Fig. 4 reveals the influence of K on $g'(0)$. The behavior of the couple stress coefficient in both solutions is the same as discussed earlier in Fig. 3. Fig. 5 interprets the impact of material parameter on $-\theta'(0)$. The enhancement in non-Newtonian parameter is caused by producing a low heat transfer rate in both solutions, as expected. Practically the negative heat transfer values indicate that heat flow from higher to lower temperature since $\delta > 0$. The effect of suction on the local Sherwood number is reported in Fig. 6.

As we know Sherwood number defines the flux rate of nanoparticle in the fluid, concentration rate of nanoparticle reduces (increases) in the first (second) solution when the material parameter is enhanced. The effect of micropolar parameter K on velocity profile is captured in Fig. 7
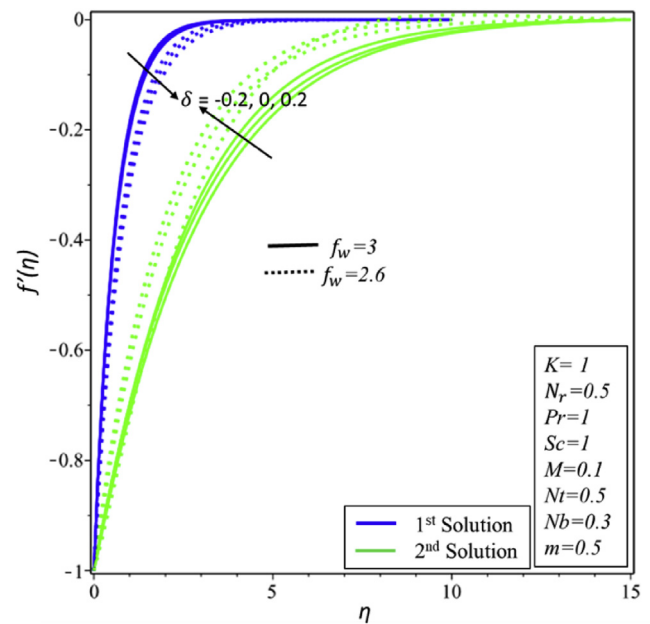

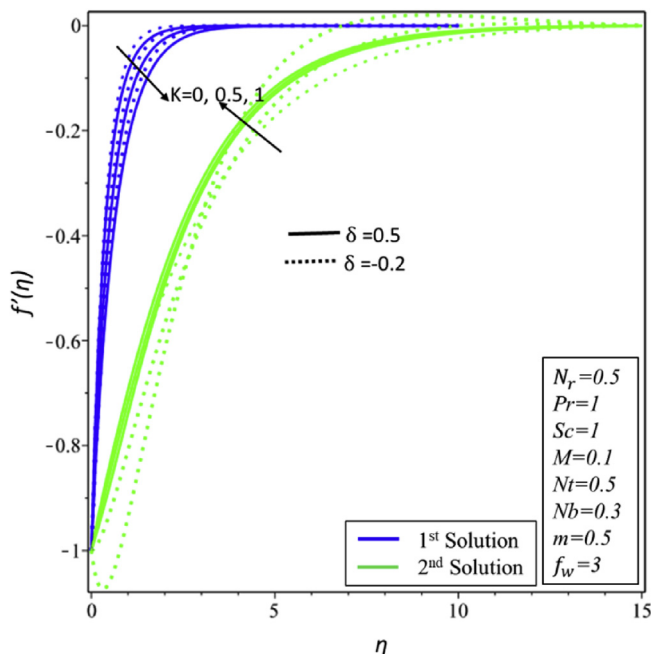**Fig. 8.** Effect of δ on velocity profile.
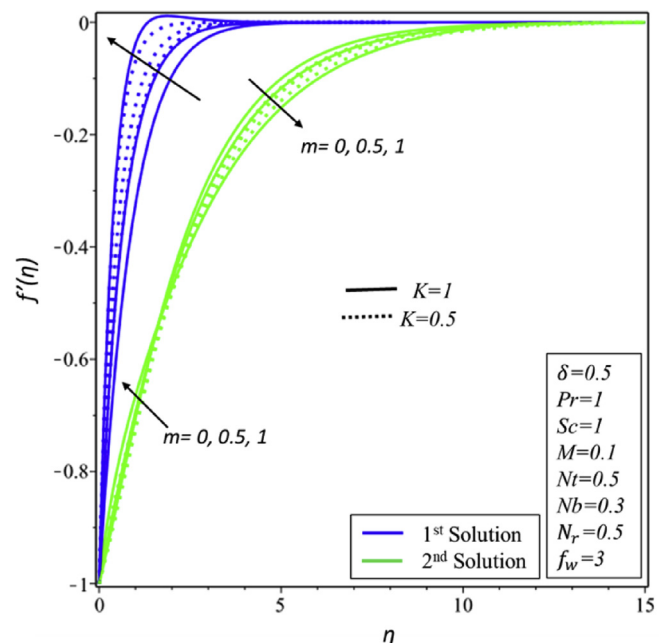

Fig. 7. Effect of K on velocity profile.
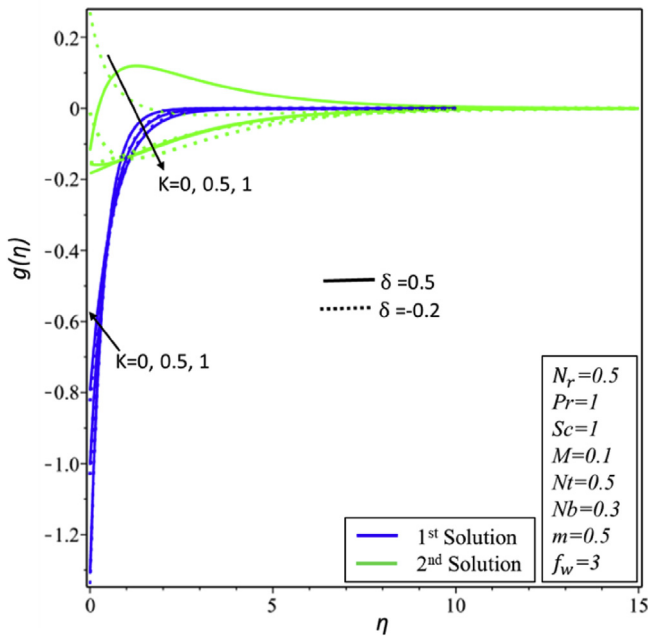

Fig. 9. Effect of m on velocity profile.

Fig. 10. Effect of K on angular velocity profile.

Fig. 12. Effect of δ on temperature profile.

where the fluid motion is directly proportional to the escalating values of K in the first solution. On the other hand, opposite behavior of velocity of fluid can be deducted in the second solution which means that the dynamic viscosity has a direct relation with material parameter. Fig. 8 was sketched to see the impact of Richardson number on the velocity profile. When δ is increased, the reduction of the velocity of micropolar nanofluid occurs in the second solution. For the first solution, the buoyancy force acts as a favorable pressure gradient. A stronger buoyancy force assists the flow in the upward direction due to its effect on the increment on momentum boundary layer. It is worth to mention that $\delta < 0$ represents the opposing flow regime, while $\delta > 0$ indicates the assisting flow case. The effect of a parameter of micro-gyration m on the velocity of fluid flow is shown in Fig. 9. The motion of fluid and thickness of the hydrodynamic boundary layer reduce as m is expanding from 0 to 1 in the first solution.
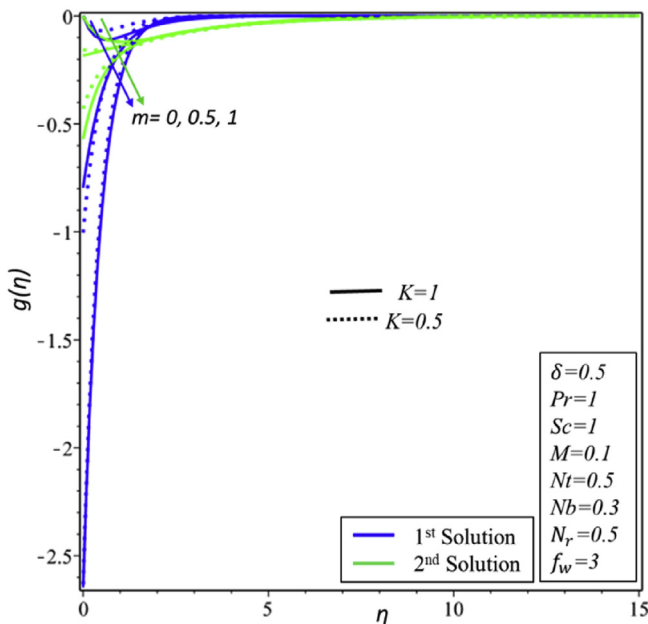
On the other side, the dual behavior of velocity profile can be seen in the second solution. Fig. 10 shows that the micropolar material parameter is directly proportional to the angular velocity of fluid motion in both solutions.

Fig. 11 depicts the effect of micro-gyration parameter m on angular velocity distribution. Both solutions have a direct relation with micro-gyration parameter m. It should be noted that the value $m = 0$ indicates that there is a strong concentration of micropolar particles. This implies that the particles are unable to rotate when they are very close to the shrinking surface. The weak concentration of particle is observed when the value of $m = 0.5$ in which the symmetrical part of the stress tensor vanishes. On the other hand, when $m = 1$, the particles are free to rotate, and the angular velocity component is dominant on micro-gyration parameter m which causes turbulent boundary layer flow. Fig. 12 depicts the effect of Richardson number on temperature
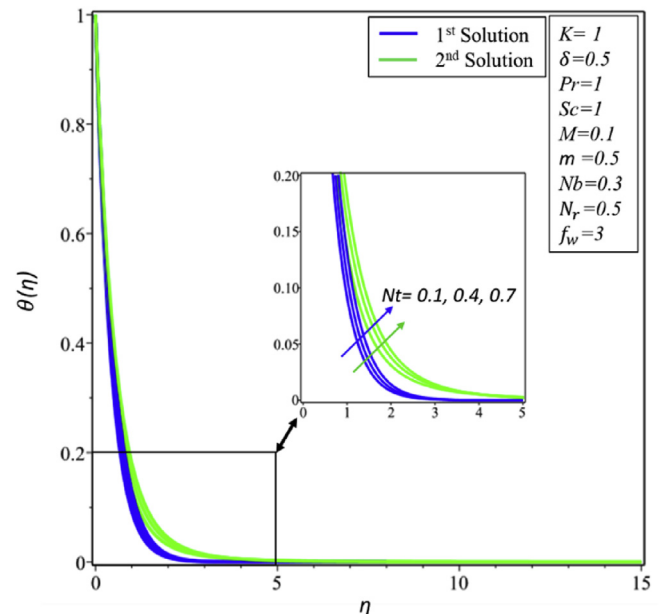

Fig. 11. Effect of m on angular velocity profile.

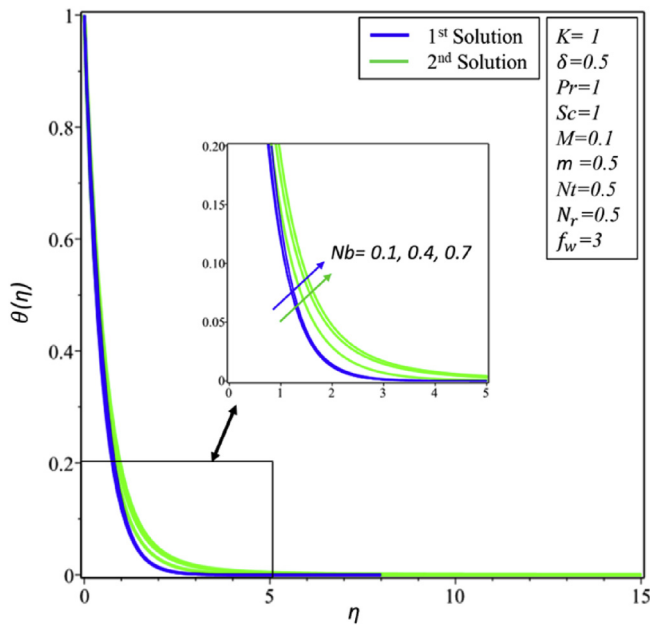**Fig. 13.** Effect of N_t on temperature profile.

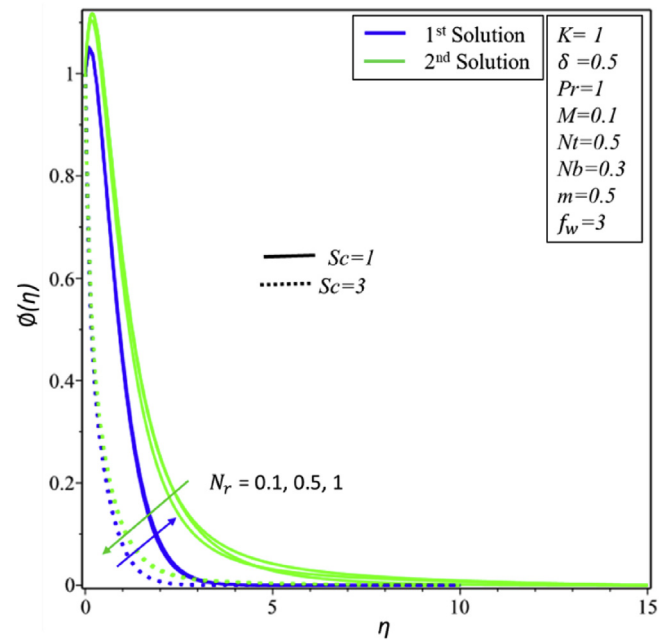**Fig. 14.** Effect of N_b on temperature profile.

Fig. 16. Effect of N_r on concentration profile.

distribution. It is found that the Richardson number δ has also some direct effects on the momentum equation. There is a slight growth in the thermal boundary layer in the first solution when δ is enhanced. Similarly, the thickness of thermal boundary layer is proportional to δ in the second solution. The effect of thermophoresis on the temperature profile is shown in Fig. 13. The thickness of thermal boundary layer enhances strictly in both solutions when N_t increases from 0.1 to 0.7. This is due to the role of thermophoresis force whereby hot nanoparticles that are close to the hot shrinking surface are being pushed to the cold fluid at the ambient temperature. As a result, the thermal boundary layer becomes thicker. The impact of Brownian motion parameter N_b on the temperature profile is revealed in Fig. 14. It can be seen that the thickness of the thermal layer is directly proportional to N_b in both solutions, as expected. Physically, this is due to the fact that temperature boundary layer becomes thicker. As N_b increases the motion of nanoparticles also increase

and they move away from their original places. As a result, the thermal layer enhances.

Fig. 15 shows the Prandtl number variation on temperature profile. Temperature layer declines in both solutions as the values of Pr increase. Prandtl number is the ratio of momentum diffusion to thermal diffusion which can be expressed as a ratio of the kinematic viscosity of the fluid to its thermal diffusivity. This means the higher Prandtl number, the lower thermal conductivity will be. Consequently, this causes the reduction in the thermal boundary layer thickness. The effect of N_r on concentration distribution was drawn in Fig. 16. It appears that for a large value of N_r the nanoparticle concentration profile rises in the first, but opposite trend is noticed for the second solution. Fig. 17 is portrayed to analyze the effect of thermophoresis on concentration distribution. The results of nanoparticles concentration profiles reveal that distribution and
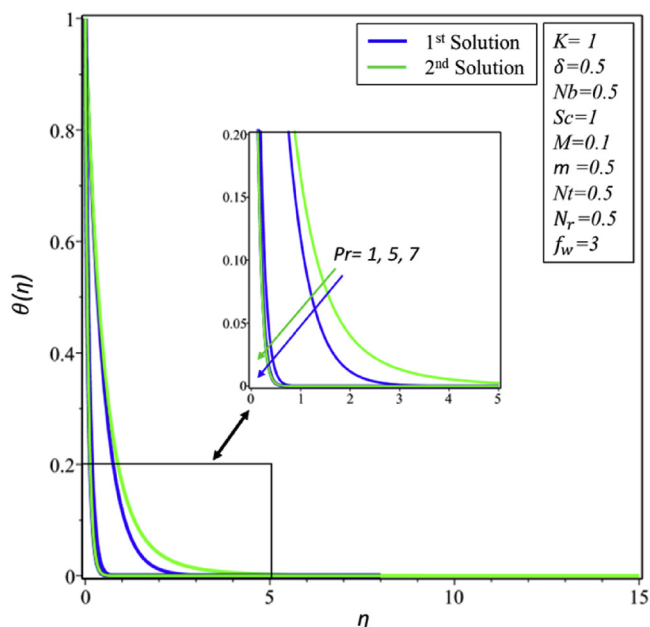

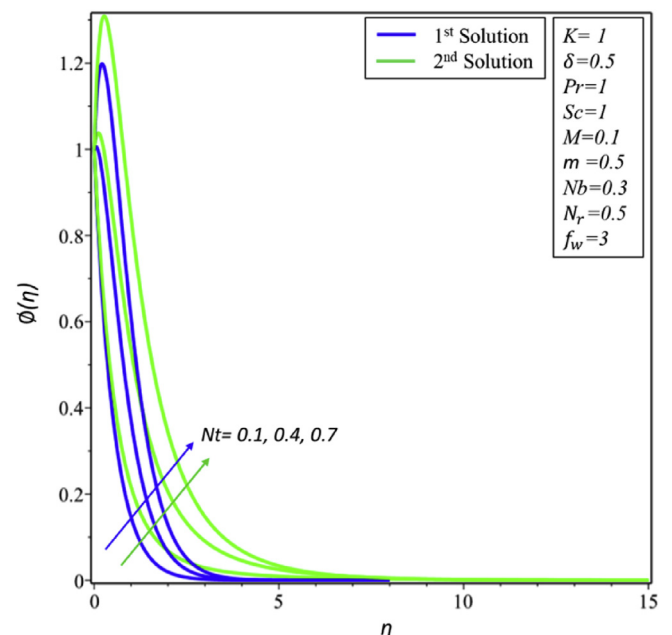**Fig. 15.** Effect of Pr on temperature profile.

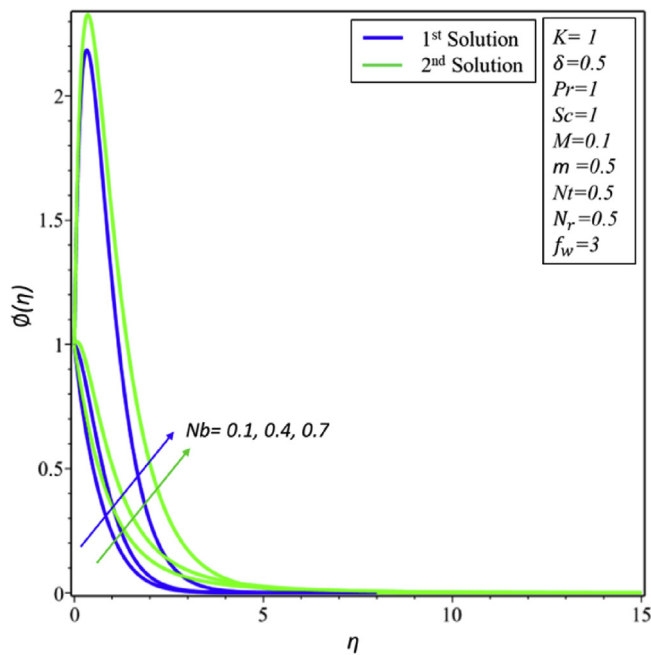**Fig. 17.** Effect of N_t on concentration profile.

Fig. 18. Effect of N_b on concentration profile.

thermophoresis parameter are directly proportional. Fig. 18 shows that the nanoparticle concentration boundary layer thickness develops when the Brownian motion strength increases in the both solutions. Fig. 19 highlights the influence of Sc on nanoparticles volume fraction profiles. As Schmidt number steadily expands, the coefficient of Brownian diffusion declines. This will eventually diminish the thickness of boundary layer in both solutions.

To perform stability analysis of dual solutions, we solved Eqs. (31), (32), (33), and (34) with boundary relaxed boundary conditions by using the three-stage Lobatto IIIa formula in MATLAB software. It is noticed that positive (negative) results of smallest eigenvalue show the stable (unstable) solution, which is the first (second) solution. It should be noted that only stable solution can be seen experimentally or used in any practical applications. For the selected parameters, where the values of
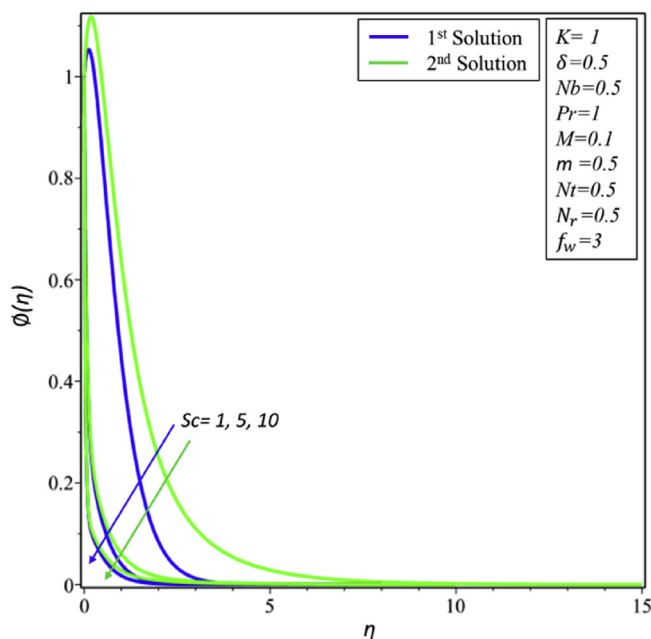

Fig. 19. Effect of Sc on concentration profile.

Table 1
Smallest eigen values for different values of K and m for δ.

K	m	δ	ε_1	
			1st solution	2nd solution
0	0	-0.2	0.35736	-1.15524
		0.2	0.49821	-0.90825
	0.5	-0.2	0.35724	-1.1345
		0.2	0.50261	-0.93417
0.5	0.5	-0.2	1.02853	-1.42019
		0.2	0.78992	-1.1542
	1	0.2	1.3182	-1.62851

parameters are $M = 0.5, N_r = 0; Pr = 1, N_b = 0.3, N_t = 0.5, and Sc = 1$, the smallest eigenvalues are founded and presented in Table 1.

5. Conclusion

Micropolar nanofluid over a vertical permeable shrinking surface is investigated. Thermophoresis, Brownian motion, and magnetic parameters effect have been included. The governing equations are converted to a system of coupled nonlinear ODEs. ODEs are tackled numerically by using shooting method. Following the main conclusion of the present study are as follow:

1. Dual solutions occur for $K = 0, 0.5 and 1$, when the range of $f_w < 2.1785, 2.3479 and 2.5103$ respectively.
2. No solution exists when the shrinking surface is impermeable.
3. Only first (Upper) solution is stable and physically possible.
4. Dual solutions exist in both cases namely opposing and assisting flow case.
5. The temperature rises in both solutions for the strong effect of Brownian motion.
6. Thermophoresis and concentration parameters are directly proportional to temperature and concentrations profiles.

Declarations

Author contribution statement

Ilyas Khan: Contributed analysis tools or data; Wrote the paper.
Zurni Omar: Analyzed and interpreted the data.
Liaquat Ali Lund: Conceived and designed the analysis.

Competing interest statement

The authors declare no conflict of interest.

Additional information

No additional information is available for this paper.

References

[1] T. Hayat, M.I. Khan, M. Waqas, A. Alsaedi, M.I. Khan, Radiative flow of micropolar nanofluid accounting thermophoresis and Brownian moment, Int. J. Hydrogen Energy 42 (26) (2017) 16821–16833.
[2] A.C. Eringen, Simple micropolar fluids, Int. J. Eng. Sci. 2 (1964).
[3] A.C. Eringen, Theory of micropolar fluids, J. Math. Mech. 16 (1966) 1–18.
[4] G. Lukaszewicz, Micropolar Fluids: Theory and Applications, Brikhauser Basel, 1999.
[5] S. Dero, A.M. Rohni, A. Saaban, MHD Micropolar Nanofluid Flow over an Exponentially Stretching/Shrinking Surface: Triple Solutions, 2019.

[6] R.A. Damseh, M.Q. Al-Odat, A.J. Chamkha, B.A. Shannak, Combined effect of heat generation or absorption and first-order chemical reaction on micropolar fluid flows over a uniformly stretched permeable surface, Int. J. Therm. Sci. 48 (8) (2009) 1658–1663.

[7] A.J. Chamkha, R.A. Mohamed, S.E. Ahmed, Unsteady MHD natural convection from a heated vertical porous plate in a micropolar fluid with Joule heating, chemical reaction and radiation effects, Meccanica 46 (2) (2011) 399–411.

[8] E. Magyari, A.J. Chamkha, Combined effect of heat generation or absorption and first-order chemical reaction on micropolar fluid flows over a uniformly stretched permeable surface: the full analytical solution, Int. J. Therm. Sci. 49 (9) (2010) 1821–1828.

[9] N.F.M. Noor, R.U. Haq, S. Nadeem, I. Hashim, Mixed convection stagnation flow of a micropolar nanofluid along a vertically stretching surface with slip effects, Meccanica 50 (8) (2015) 2007–2022.

[10] R.U. Haq, S. Nadeem, N.S. Akbar, Z.H. Khan, Buoyancy and radiation effect on stagnation point flow of micropolar nanofluid along a vertically convective stretching surface, IEEE Trans. Nanotechnol. 14 (1) (2015) 42–50.

[11] M.E.M. Khedr, A.J. Chamkha, M. Bayomi, MHD flow of a micropolar fluid past a stretched permeable surface with heat generation or absorption, Nonlinear Anal. Model Control 14 (1) (2009) 27–40.

[12] M.M. Rashidi, M. Reza, S. Gupta, MHD stagnation point flow of micropolar nanofluid between parallel porous plates with uniform blowing, Powder Technol. 301 (2016) 876–885.

[13] M. Turkyilmazoglu, Free and circular jets cooled by single phase nanofluids, Eur. J. Mech. B Fluid 76 (2019) 1–6.

[14] M. Turkyilmazoglu, Flow of a micropolar fluid due to a porous stretching sheet and heat transfer, Int. J. Non-Linear Mech. 83 (2016) 59–64.

[15] M. Turkyilmazoglu, A note on micropolar fluid flow and heat transfer over a porous shrinking sheet, Int. J. Heat Mass Transf. 72 (2014) 388–391.

[16] L.J. Crane, Flow past a stretching plate, ZAMP (Z. Angew. Math. Phys.) 21 (1970) 645–647.

[17] P. Carragher, L.J. Crane, Heat transfer on a continuous stretching sheet, ZAMM-J. Appl. Math. Mech./Zeitschrift für Angewandte Mathematik und Mechanik 62 (10) (1982) 564–565.

[18] M. Miklavčič, C.Y. Wang, Viscous flow due to a shrinking sheet, Q. *Appl. Math.* 64 (2006) 283–290.

[19] L.A. Lund, Z. Omar, I. Khan, Analysis of dual solution for MHD flow of Williamson fluid with slippage, Heliyon 5 (3) (2019), e01345.

[20] R.S.R. Gorla, A. Chamkha, Natural convective boundary layer flow over a nonisothermal vertical plate embedded in a porous medium saturated with a nanofluid, Nanoscale Microscale Thermophys. Eng. 15 (2) (2011) 81–94.

[21] L.A. Lund, Z. Omar, I. Khan, J. Raza, M. Bakouri, I. Tlili, Stability analysis of Darcy-Forchheimer flow of casson type nanofluid over an exponential sheet: investigation of critical points, Symmetry 11 (3) (2019) 412.

[22] A.J. Chamkha, A.R.A. Khaled, Hydromagnetic combined heat and mass transfer by natural convection from a permeable surface embedded in a fluid-saturated porous medium, Int. J. Numer. Methods Heat Fluid Flow 10 (5) (2000) 455–477.

[23] D. Sumera, J. Uddin, A. Rohni, Stefan blowing and slip effects on unsteady nanofluid transport past a shrinking sheet: multiple solutions, Heat Transf. Asian Res. (2019).

[24] P.S. Reddy, P. Sreedevi, A.J. Chamkha, MHD boundary layer flow, heat and mass transfer analysis over a rotating disk through porous medium saturated by Cu-water and Ag-water nanofluid with chemical reaction, Powder Technol. 307 (2017) 46–55.

[25] P.S. Reddy, A.J. Chamkha, Soret and Dufour effects on MHD convective flow of Al2O3–water and TiO2–water nanofluids past a stretching sheet in porous media with heat generation/absorption, Adv. Powder Technol. 27 (4) (2016) 1207–1218.

[26] A. Al-Mudhaf, A.J. Chamkha, Similarity solutions for MHD thermosolutal Marangoni convection over a flat surface in the presence of heat generation or absorption effects, Heat Mass Transf. 42 (2) (2005) 112–121.

[27] A.J. Chamkha, S. Abbasbandy, A.M. Rashad, K. Vajravelu, Radiation effects on mixed convection about a cone embedded in a porous medium filled with a nanofluid, Meccanica 48 (2) (2013) 275–285.

[28] C. RamReddy, P.V.S.N. Murthy, A.J. Chamkha, A.M. Rashad, Soret effect on mixed convection flow in a nanofluid under convective boundary condition, Int. J. Heat Mass Transf. 64 (2013) 384–392.

[29] S.U. Choi, J.A. Eastman, Enhancing thermal Conductivity of Fluids with Nanoparticles (No. ANL/MSD/CP-84938; CONF-951135-29), Argonne National Lab., IL (United States), 1995.

[30] O. Mahian, L. Kolsi, M. Amani, P. Estellé, G. Ahmadi, C. Kleinstreuer, et al., Recent Advances in Modeling and Simulation of Nanofluid Flows-Part I: Fundamental and theory. Physics Reports, 2018.

[31] J. Buongiorno, Convective transport in nanofluids, J. Heat Transf. 128 (3) (2006) 240–250.

[32] R.K. Tiwari, M.K. Das, Heat transfer augmentation in a two-sided lid-driven differentially heated square cavity utilizing nanofluids, Int. J. Heat Mass Transf. 50 (9-10) (2007) 2002–2018.

[33] M. Turkyilmazoglu, Buongiorno model in a nanofluid filled asymmetric channel fulfilling zero net particle flux at the walls, Int. J. Heat Mass Transf. 126 (2018) 974–979.

[34] E. Magyari, A.J. Chamkha, Exact analytical results for the thermosolutal MHD Marangoni boundary layers, Int. J. Therm. Sci. 47 (7) (2008) 848–857.

[35] A.J. Chamkha, A.M. Rashad, T. Armaghani, M.A. Mansour, Effects of partial slip on entropy generation and MHD combined convection in a lid-driven porous enclosure saturated with a Cu–water nanofluid, J. Therm. Anal. Calorim. 132 (2) (2018) 1291–1306.

[36] M. Sheikholeslami, CuO-water nanofluid flow due to magnetic field inside a porous media considering Brownian motion, J. Mol. Liq. 249 (2018) 921–929.

[37] N.F.M. Razali, A. Fudholi, M.H. Ruslan, K. Sopian, Review of water-nanofluid based photovoltaic/thermal (PV/T) systems, Int. J. Electr. Comput. Eng. 9 (1) (2019) 134–140.

[38] G.C. Bourantas, V.C. Loukopoulos, Modeling the natural convective flow of micropolar nanofluids, Int. J. Heat Mass Transf. 68 (2014) 35–41.

[39] G.C. Bourantas, V.C. Loukopoulos, MHD natural-convection flow in an inclined square enclosure filled with a micropolar-nanofluid, Int. J. Heat Mass Transf. 79 (2014) 930–944.

[40] J.C. Umavathi, J.P. Kumar, A.J. Chamkha, I. Pop, Mixed convection in a vertical porous channel, Transp. Porous Media 61 (3) (2005) 315–335.

[41] H.S. Takhar, A.J. Chamkha, G. Nath, Unsteady mixed convection flow from a rotating vertical cone with a magnetic field, Heat Mass Transf. 39 (4) (2003) 297–304.

[42] A.J. Chamkha, C. Issa, K. Khanafer, Natural convection from an inclined plate embedded in a variable porosity porous medium due to solar radiation, Int. J. Therm. Sci. 41 (1) (2002) 73–81.

[43] A.J. Chamkha, Coupled heat and mass transfer by natural convection about a truncated cone in the presence of magnetic field and radiation effects, Numer. Heat Transf. Part A: Applications 39 (5) (2001) 511–530.

[44] A.J. Chamkha, Solar radiation assisted natural convection in uniform porous medium supported by a vertical flat plate, J. Heat Transf. 119 (1) (1997) 89–96.

[45] J.H. Merkin, On dual solutions occurring in mixed convection in a porous medium, J. Eng. Math. 20 (2) (1986) 171–179.

[46] L.A. Lund, Z. Omar, I. Dero, Multiple solutions of Cu-C 6 H 9 NaO 7 and Ag-C 6 H 9 NaO 7 nanofluids flow over nonlinear shrinking surface, J. Cent. South Univ. 26 (5) (2019) 1283–1293.

[47] I.M. Alarifi, A.G. Abokhalil, M. Osman, L.A. Lund, M.B. Ayed, H. Belmabrouk, I. Tlili, MHD flow and heat transfer over vertical stretching sheet with heat sink or source effect, Symmetry 11 (3) (2019) 297.

[48] K. Bhattacharyya, S. Mukhopadhyay, G.C. Layek, I. Pop, Effects of thermal radiation on micropolar fluid flow and heat transfer over a porous shrinking sheet, Int. J. Heat Mass Transf. 55 (11-12) (2012) 2945–2952.